

Figure S1. Kinetics of **(A)** f-WT and **(B)** f-F3A fibrillation followed by ThT fluorescence, at 37°C and varying peptide concentrations. Error bars stand for the standard deviation between three replicates.

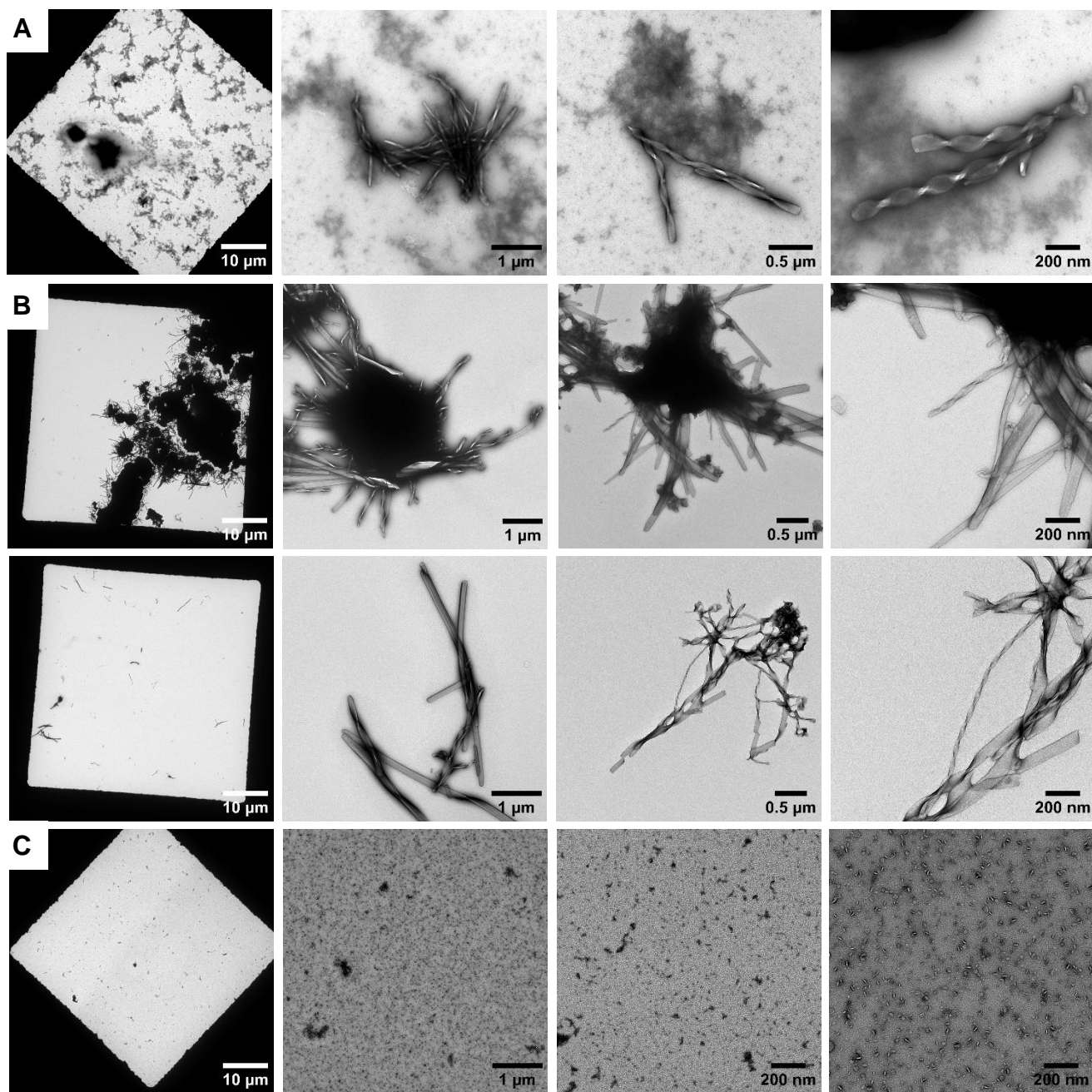


Figure S2. Negatively stained TEM images of **(A-B)** f-WT and **(C)** f-F3A peptides obtained after 3 days incubation at 37°C. (A) f-WT and (C) f-F3A were deposited per se, in buffer conditions. (B) f-WT were centrifuged, and the pellet resuspended in ultrapure water, to properly imaged the mature fibrils only. Two types of areas were observed, with f-WT fibrils highly clustered into large bundles (top) or small clusters with even isolated fibrils (bottom).

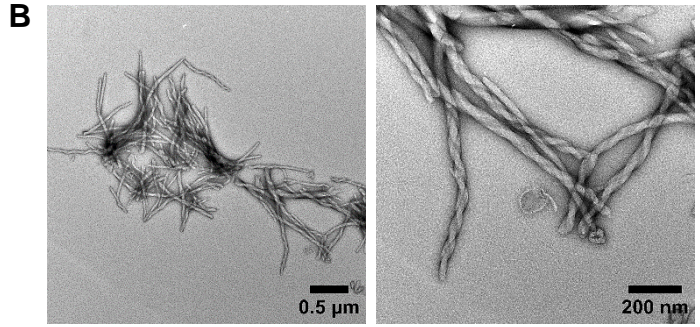
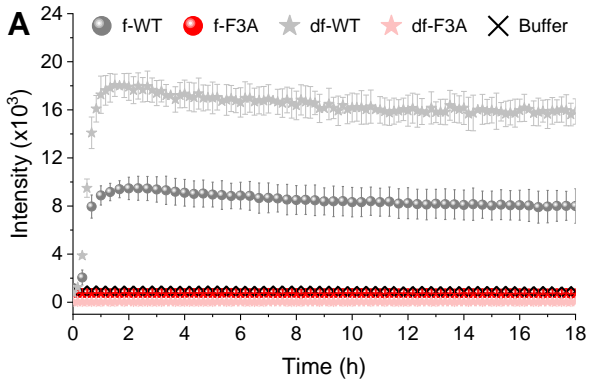
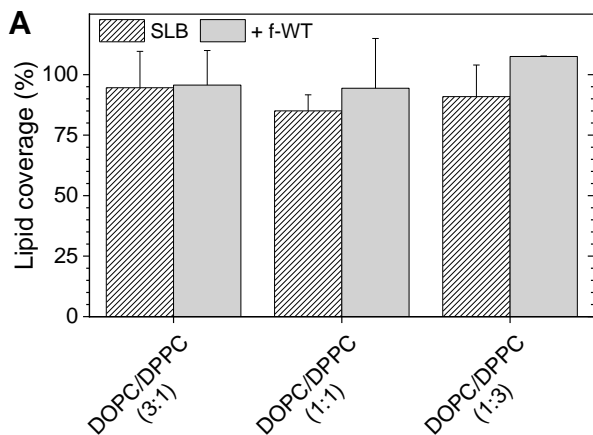


Figure S3. (A) Comparison of the fibril formation of formylated (f-) and deformed (df-) PSM α 3 followed by ThT fluorescence (37°C, peptide concentration 50 μM). Error bars stand for the standard deviation between three replicates. **(B)** Negatively stained TEM images of df-WT fibrils obtained after 3 days incubation at 37°C.



B

	f-WT	$\nu_{as}(\text{CH}_2)$ (cm^{-1})	$R_{\text{ATR}}(\nu_{as}(\text{CH}_2))$
DOPC / DPPC (3:1)	-	2922	1.26 ± 0.11
	+	2923	1.26 ± 0.07
DOPC/DPPC (1:1)	-	2920	1.20 ± 0.08
	+	2921	1.36 ± 0.15
DOPC/DPPC (1:3)	-	2919	1.35 ± 0.13
	+	2919	1.35 ± 0.08

Figure S4. (A) Lipid coverage of the ATR-FTIR sensor, determined *via* the variations in $\nu_{as}(\text{CH}_2)$ intensity, for binary DOPC/DPPC SLB, with varying concentration of DPPC, and following f-WT addition (3 h, 10 μM). Results are presented as mean \pm standard deviation of at least three independent replicates. **(B)** Table of the wavenumber and dichroic ratio of the CH_2 of DOPC/DPPC membranes with varying ratio of DPPC, before (-) and after (+) f-WT addition at 10 μM for 3h. Analyzed spectra were obtained in the *p*-polarization.

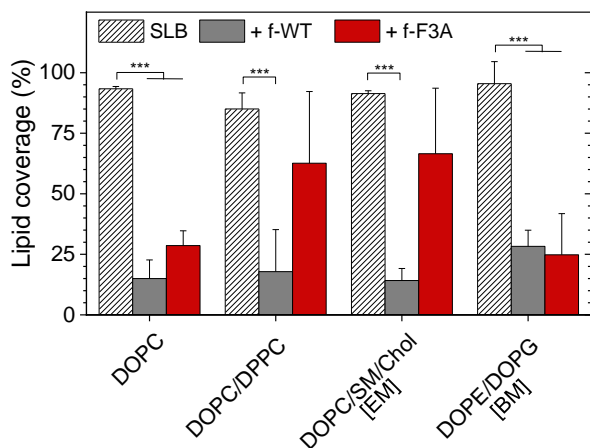


Figure S5. Lipid coverage of the ATR-FTIR sensor, determined *via* the variations in $\nu_{as}(\text{CH}_2)$ intensity, for SLB of diverse composition following PSM α 3 incubation for 1 h at 50 μM . Results are presented as mean \pm standard deviation of at least three independent replicates. *** $p < 0.001$. Analyzed spectra were obtained in the p -polarization. EM: eukaryotic mimetic membrane, BM: bacterial mimetic membrane.

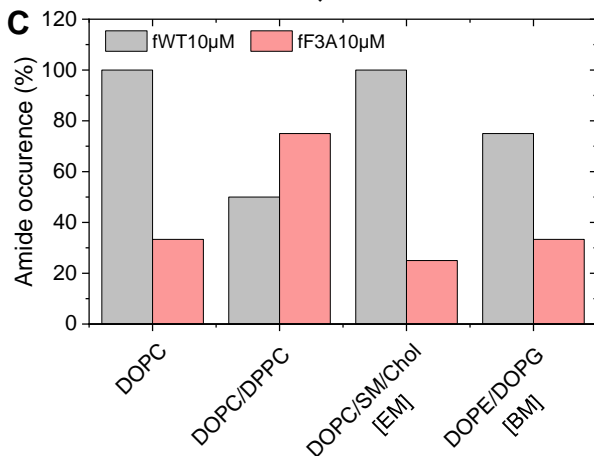
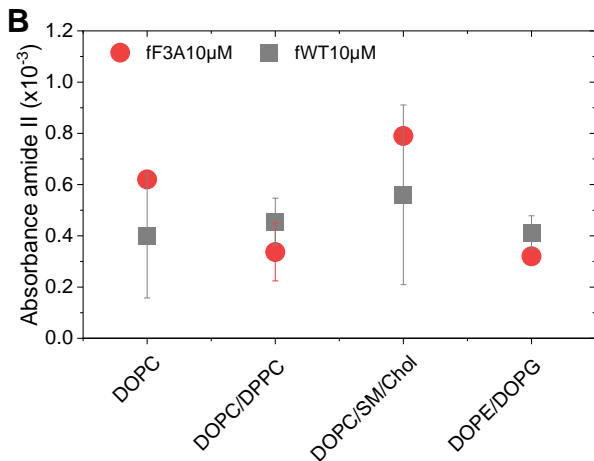
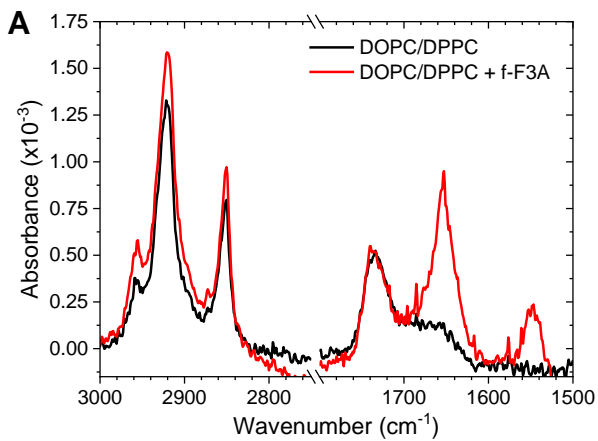


Figure S6. Quantification of PSM α 3 deposition at the SLB interface. (A) ATR-FTIR spectra (*p-pol*) of a DOPC/DPPC SLB before and after a 3 h incubation with f-F3A at 10 μ M, illustrating the accumulation of the peptides at the membrane interface (Amide I and II observable). **(B)** Absolute intensities, in the *p-pol*, of the Amide II band (~ 1550 cm^{-1}) after a 3h incubation of PSM α 3 (f-WT and f-F3A) on SLB of different compositions. **(C)** Deposition occurrence of PSM α 3, estimated by the ratio between the number of spectra featuring the Amide I and II bands and the total number of spectra recorded. EM: eukaryotic mimetic membrane, BM: bacterial mimetic membrane.

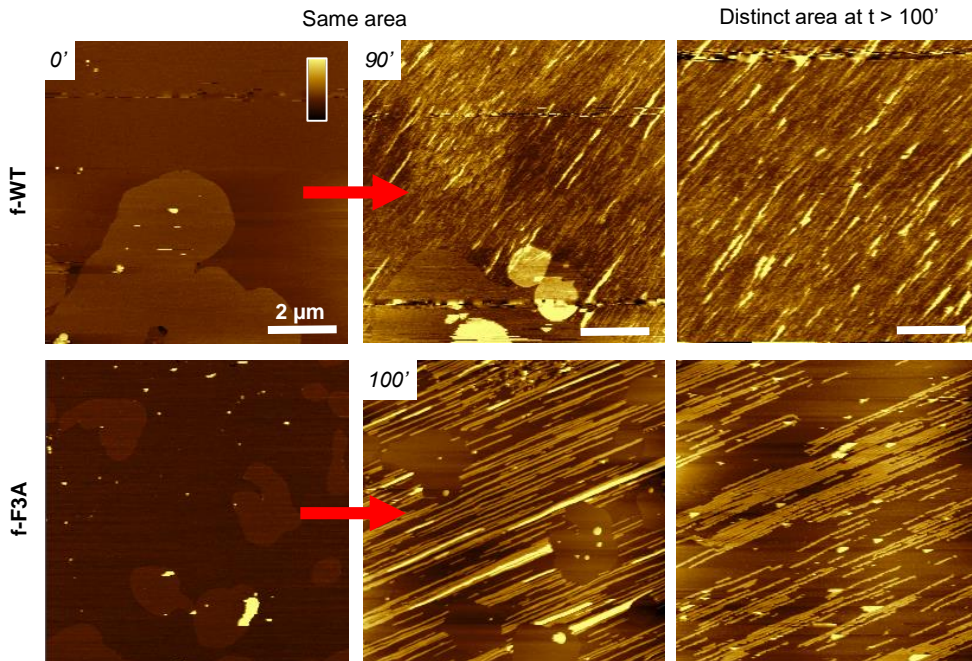


Figure S7. Fibrillation of f-PSM α 3 (WT and F3A) at the membrane interface (here, exemplified with DOPC/DPPC (1:1)) is independent of the AFM-tip scanning. Similar fibrils were always observed in areas different from those scanned in real-time. Color scale bars: 15nm.

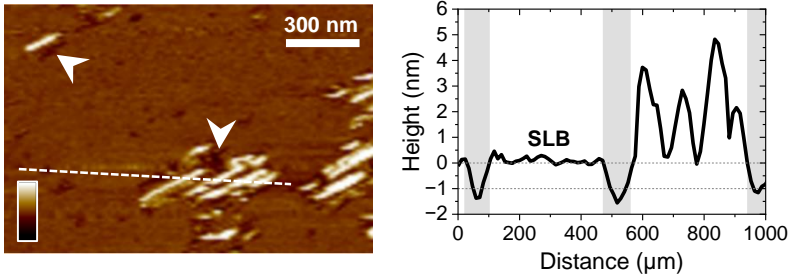


Figure S8. Topographical analysis of a DOPC/SM/Chol membrane interacting with f-WT (5 μM). The AFM topography image and the corresponding height profile along the dashed line showcase short fibrils (~ 5 nm) surrounded by areas thinner than the SLB (white arrows and grey area). Small holes can also be observed in the membrane, independently of the f-WT presence. Color scale bar: 10 nm.

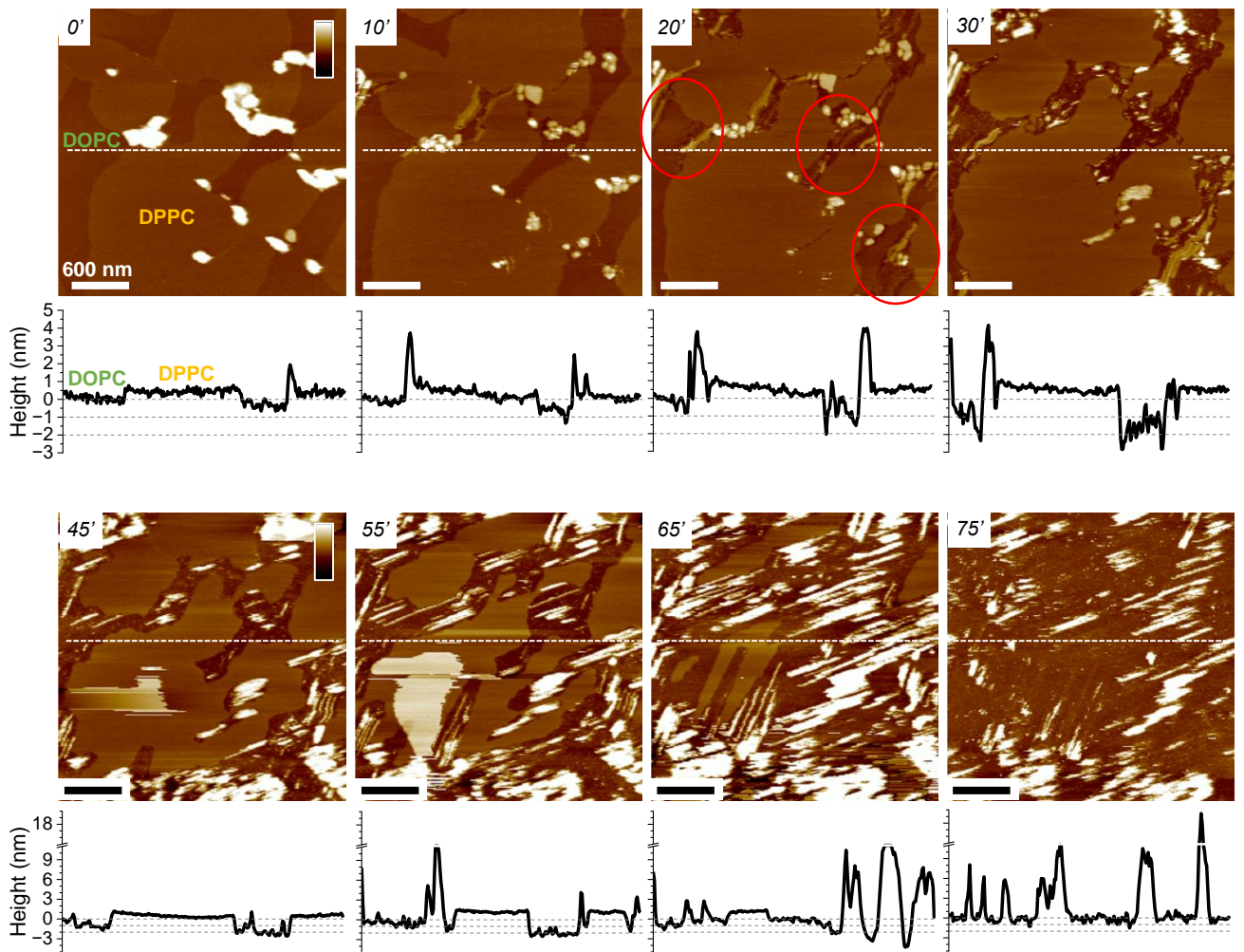


Figure S9. Topographical analysis of a DOPC/DPPC membrane interacting with f-WT at a concentration of $15\mu\text{M}$, at representative timepoints. Height profiles along the dashed lines in the AFM topography images are shown to quantitatively measure membrane damage and peptide aggregation. Red circles point to areas where membrane thinning starts occurring (from 1 to 2 nm), as also shown by the height profiles over time.

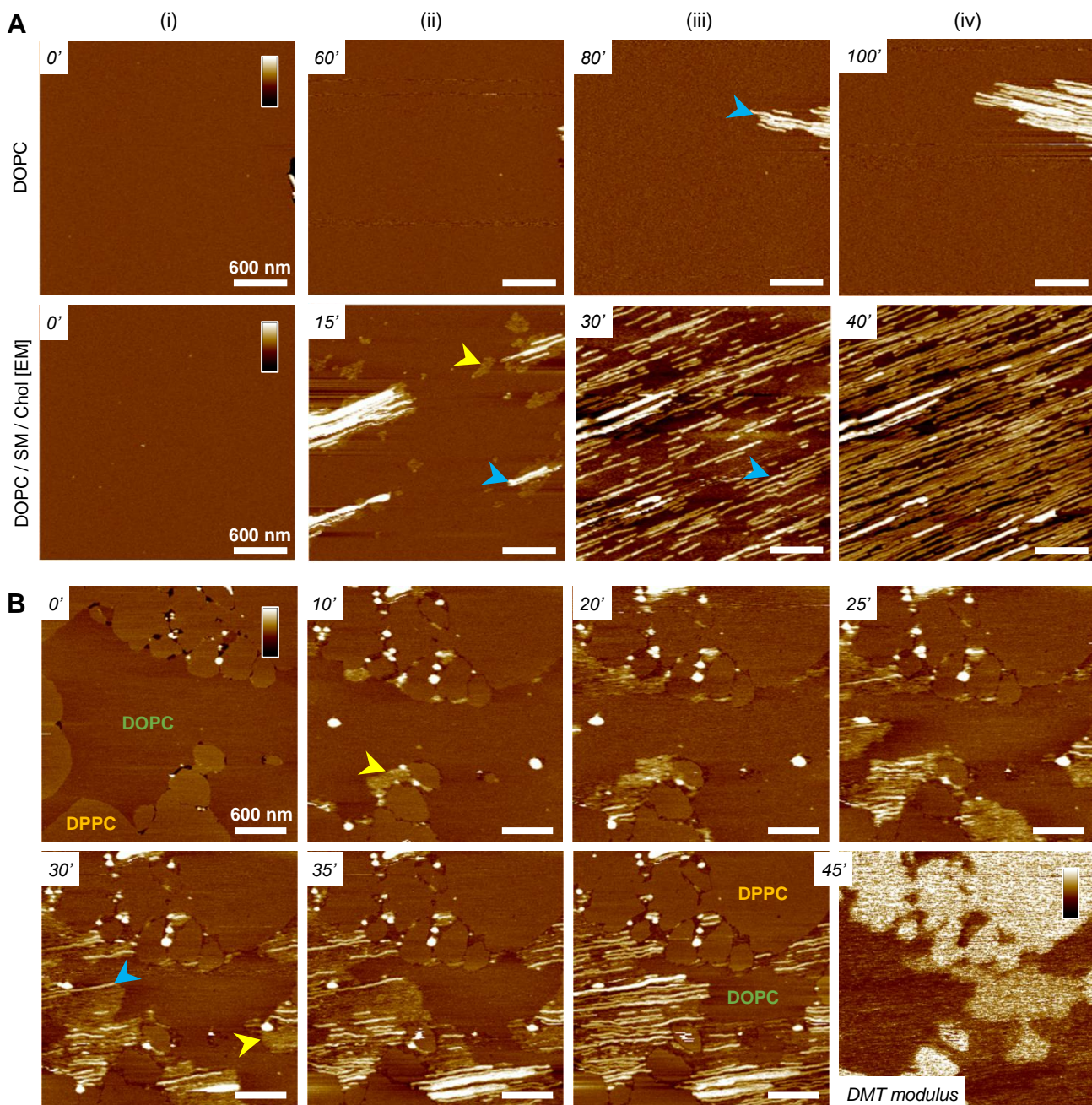


Figure S10. Fibrillation of f-F3A PSM α 3 on DOPC-containing membranes. (A) AFM topography images, at representative timepoints, of various DOPC-containing SLB interacting with 5 μ M f-F3A. After a lag-time during which the SLB remains intact (i), small aggregates (ii - yellow arrows) first appear before elongating as thin fibrils (iii - blue arrows), covering a larger and larger proportion of the membrane (iv). EM: eukaryotic mimetic membrane. **(B)** Timelapse of the growth of both protofibrils (yellow arrows) and mature fibrils (blue arrows) of f-F3A in the fluid DOPC phase of a binary DOPC/DPPC SLB. The front of protofibrils is further evidenced by their mechanical properties (DMT modulus image at 45min of incubation), softer than the surrounding membrane. Color scale bars: 10nm, 2 log(Pa).

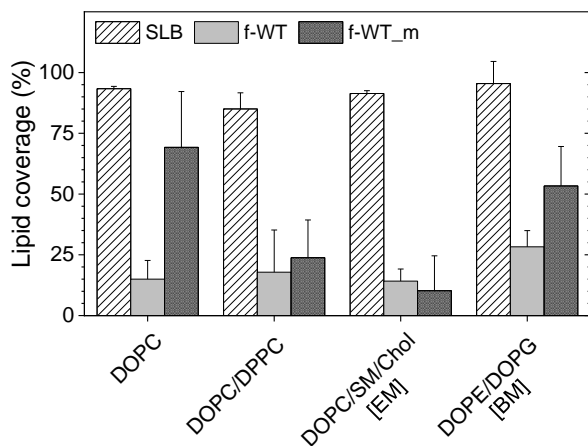


Figure S11. Lipid coverage of the ATR-FTIR sensor, determined *via* the variations in $\nu_{as}(\text{CH}_2)$ intensity, for SLB of diverse composition following f-WT incubation at $50 \mu\text{M}$ for 1 h, injected as a fibrillated solution (3 days at 37°C , f-WT) or an initial monomeric solution (f-WT_m). Results are presented as mean \pm standard deviation of at least three independent replicates. Analyzed spectra were obtained in the p -polarization. EM: eukaryotic mimetic membrane, BM: bacterial mimetic membrane.